This article has been accepted for publication in IEEE Journal of Electromagnetics, RF and Microwaves in Medicine and Biology. This is the author's version which has not been fully edited content may change prior to final publication. Citation information: DOI 10.1109/JERM.2022.3205847

Electromagnetic-Based Deformation Monitoring for PANI-CA Breath Acetone Sensors

Balaji Dontha, *Student Member*, IEEE, Asimina Kiourti, *Senior Member*, IEEE

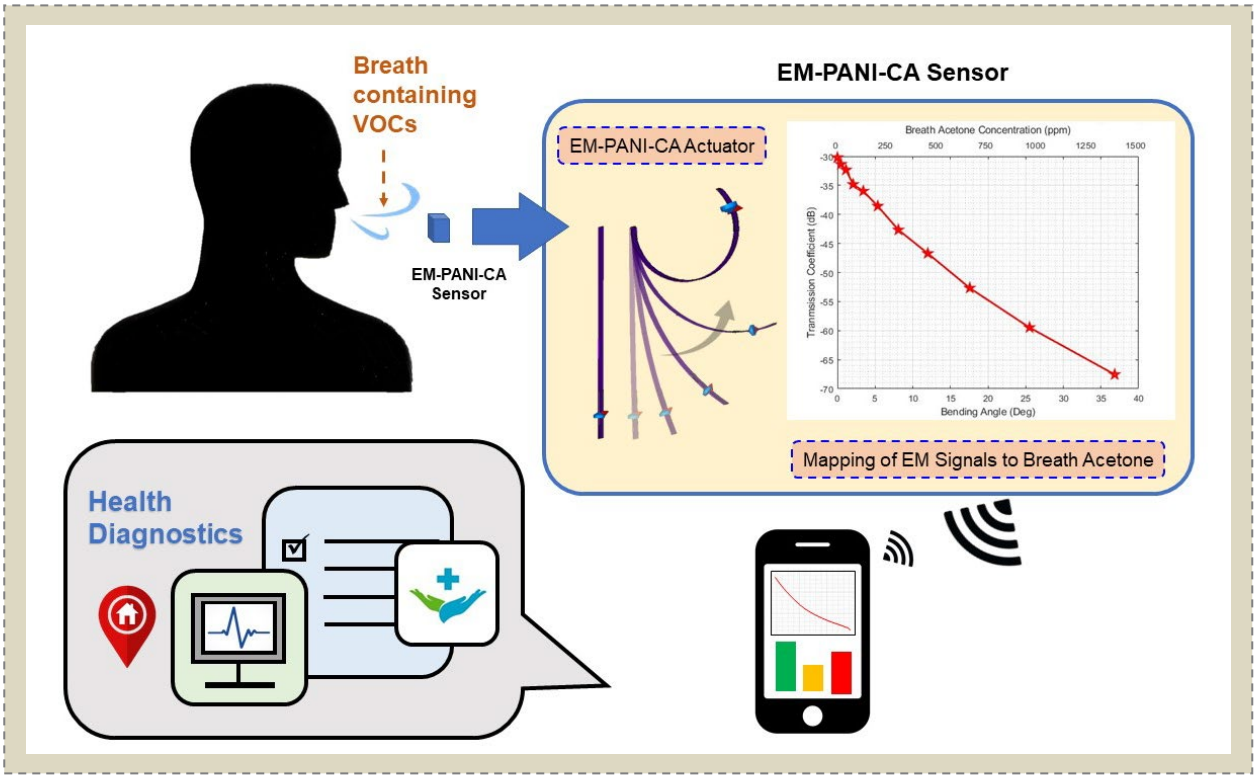

An electromagnetic (EM) approach to monitoring deformation of chemo-actuating PANI-CA strips towards breath acetone sensing for smart health diagnostics.

Take-Home Messages

- We report a novel electromagnetic-based sensing mechanism for quantifying naturally released acetone from the human breath.
- The proposed technique may be used to continuously monitor acetone levels at ambient temperature and can be ultimately integrated into a wearable device with a detection limit of 1 ppm.
- This technology can be used for various health diagnostics, such as fat metabolism, weight loss, type 2 diabetes, and ketosis.
- The sensor designed using this electromagnetic approach can be ultimately integrated in a continuous, non-invasive, and personalized device that covers the entire breath acetone range.

Electromagnetic-Based Deformation Monitoring for PANI-CA Breath Acetone Sensors

Balaji Dontha, *Student Member*, IEEE, Asimina Kiourti, *Senior Member*, IEEE

Abstract We report a novel electromagnetic (EM) based mechanism for quantifying bending in PANI-CA chemo-actuators that detect breath acetone and validate feasibility in a proof-of-concept *in vitro* setup. Breath acetone serves as a biomarker of human metabolism, yet previously reported techniques are invasive, non-continuous, and/or operate at high temperatures. To overcome these limitations, we rely on previously reported polyaniline and cellulose acetate (PANI-CA) chemo-actuators that are known to flex up to 30º in response to breath acetone levels (i.e., up to 1250 ppm) in a reversible process. Our approach comprises of resonant loops placed in proximity to as well as embedded in 4 cm × 3 mm PANI-CA strips and operates at room temperature. To minimize impact to the strip's mechanical performance, loops are realized on lightweight conductive threads. Using Faraday's law as the strip deforms and the loops misalign, the sensor is shown to monitor acetone-headspace concentration at a limit of detection and resolution of 26.1 ppm experimentally and 1 ppm through interpolation. We also demonstrate that our EM mechanism in conjunction with PANI-CA strips: (a) is suitable for acetone sensing up to 2610 ppm (70º flexion) relevant to other applications beyond breath, and (b) can be modified to monitor deformation of up to 170º shall more sensitive chemo-actuating strips be implemented in the future. This technology can be integrated into a wearable device for-instance mask or mouthpiece. Personalized, non-invasive and continuous sensing of acetone biomarker can bolster monitoring of various health diagnostics, such as fat-metabolism, weight loss, and ketosis.

Keywords **— Acetone sensing, chemo-actuators, conductive threads, Faraday's law, metabolic rate monitoring, resonant loops**

I. Introduction[1]

MORE than one-third of the adult population in the United States, i.e., ~97 million people, met the criteria of metabolic syndrome in 2012 [1]. Indeed, a survey conducted over the years by the National Health and Nutrition Examination shows that metabolic syndrome is prevalent in the United States and averaged at 36.9% in 2016 [2]. In turn, metabolic syndrome leads to metabolic rate disorders, such as adverse lipid concentration, hypertension, type 2 diabetes, gall bladder disease, osteoarthritis, sleep apnea, stroke, respiratory problems, and various cancers (endometrial, breast, prostate, colon) [3].

State-of-the-art metabolism monitoring techniques, such as the Comprehensive Metabolic Panel test and the Resting Metabolic Rate test, are invasive and constrained to laboratory environments, respectively. Moreover, the patient has to prepare and follow a protocol, viz. fast at least 5 hours before the test, abstain from alcohol for a minimum of 2 hours, inform the doctor about any medications being taken, and avoid exercise or drinking caffeine [4,5]. This is cumbersome and does not provide immediate results.

Recent studies have confirmed that acetone levels in the human body can be used as a biomarker of human metabolism detection and monitoring [6, 7]. Importantly, it has been established that there is a direct correlation between acetone content in the blood [8, 9] and acetone exhaled with breath [6, 10-14]. To this end, a number of human breath monitoring techniques have been explored as a means of monitoring metabolism in a non-invasive manner. Note that breath acetone concentration may range from 1 ppm in non-dieting healthy people to 1250 ppm in diabetic ketoacidosis patients [15]. Referring to Table I, example technologies include gas chromatography - mass spectrometry (GC-MS) [16], proton-transfer reaction - mass spectrometry (PTR-MS) [17], and selected ion flow tube - mass spectrometry (SIFT-MS) [18] that rely on selective analysis of volatile organic compounds (VOCs) in human breath, including acetone. However, they have several drawbacks as highlighted in [19], such as relying on bulky equipment, being limited to sparse measurements (i.e., lack of continuous monitoring), and requiring a trained operator. Other technologies, such as Quantum cascade lasers (QCLs) [20], CAES-QCL [21] and external cavity QCL [22] are usually not continuous and require laser source with complex post processing. Semiconductor metal-oxide (SMOS) sensors [23-27] rely on changes in resistivity with the sensed acetone levels, but exhibit low sensitivity and selectivity. SMOS sensors further utilize high operating temperatures (180 to 600 ºC) [28] that add to the complexity of the device, impose safety concerns, and impair the device's durability. Radio Frequency (RF)-based sensors [29-33] are also a promising area to explore for non-invasive, continuous and portable breath-based acetone sensing. Research done by [29] reports planar

Manuscript received May 23, 2022. This work was supported by the National Science Foundation under Grant 2014506.
B. Dontha and A. Kiourti are with the ElectroScience Laboratory, Dept. of Electrical and Computer Engineering, The Ohio State University, Columbus, OH, 43212 (e-mail: dontha.1@osu.edu, kiourti.1@osu.edu).

TABLE I
COMPARISON OF APPROACHES FOR BREATH ACETONE DETECTION

Method	Range (ppm)	Detection Limit (ppm)	Response Time (sec)	Operating Temp (°C)	Non Invasive	Continuous	Portable	Ref
GC–MS	0.073 – 6.64	0.049	240	~300	Yes	No	No	[16]
PTR–MS	0.013 – 2.6	0.003	1.5	-	Yes	No	No	[17]
SIFT–MS	0.148 – 2.74	>0.001	20 ms	ambient	Yes	No	No	[18]
QCL	0 – 0.9	0.030	-	ambient	Yes	No	No	[20]
CAES-QCL	0-5	0.51	0.2	ambient	Yes	No	No	[21]
EC-QCL	5-50	0.015	40	ambient	Yes	No	Yes	[22]
SMOS	1000	188	45	400	Yes	Yes	Yes	[23]
SMOS	67	11	7	380	Yes	Yes	Yes	[24]
SMOS	500	234.4	6.1	180	Yes	Yes	Yes	[25]
SMOS	10	2	9	600	Yes	Yes	Yes	[26]
SMOS	500	15.24	9.19	270	Yes	Yes	Yes	[27]
RF-based	700-2000	270	varying	ambient	Yes	Yes	Yes	[31]
RF-based	625-5000	-	-	ambient	Yes	Yes	Yes	[32]
RF-based	387-1935	165	Real Time	ambient	Yes	Yes	Yes	[33]
This Work	**1 – 2610**	**26.1**	**55**	**ambient**	**Yes**	**Yes**	**Yes**	

antenna sensor based on $Ti_3C_2T_x$ MXene membrane for monitoring of VOCs, while [30] integrates split ring resonators with graphene oxide-based P polyaniline (GO-PANI) for ammonia sensing with the potential to be used for healthcare. More recently, Ketone breathalyzers have become commercially available, e.g., from Ketonix [34], Keyto [35], and Biosense [36], among others, that rely on operating principles similar to the aforementioned semiconductor-based sensors [37]. However, these breathalyzers are again not continuous (the user needs to explicitly bring the device towards his/her mouth and exhale directly into the device), require careful handling, and are often inaccurate with varying measurement conditions.

Here, we take a major step forward and explore a new breath acetone sensing mechanism based on previously reported polyaniline and cellulose acetate (PANI-CA) chemo-actuators [38] with potential to overcome limitations in the state-of-the-art by being: (a) non-invasive, (b) continuous, (c) seamless to use, (d) operational at room temperature, and (e) robust to the measuring conditions. The new idea is to fuse the PANI-CA strips with EM technology and map their deformation into breath acetone levels (Section II). To this end, we embed resonant loops and use Faraday's law of induction to relate loop displacement to acetone headspace concentration. PANI-CA composite is essential to the functioning of our sensor and is known to bend up to 30º in response to breath acetone levels (i.e., up to 1250 ppm) in a reversible process [38]. We replicate deformations reported in [38] in microwave simulations and prove the concept using *in vitro* environments emulating realistic conditions. We optimize the EM deformation sensing mechanism for maximum sensitivity and use fine/lightweight conductive threads (e-threads) to form the loops such that natural motion of bending is preserved. We further demonstrate that the sensor: (a) is suitable for acetone sensing up to 2610 ppm (70º flexion per [38]) as relevant to other applications beyond breath (Section III), and (b) can be modified to monitor deformation of up to 170º shall more sensitive chemo-actuating strips be implemented in the future (Section IV). Finally, we discuss the sensor's robustness to surrounding dielectrics (chemo-actuating strip,

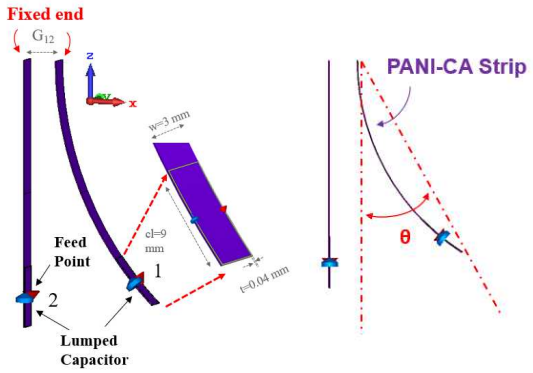

(a) (b)

Angle (θ)	0°	12°	24°	33°	46°	62°	68°
Conc (ppm)	0	525	1050	1600	2150	2325	2610

Fig. 1. Overview of EM-functionalized PANI-CA actuator for breath acetone sensing: (a) schematic, and (b) bending vs. time. All data are obtained from [38].

biological tissues) and its Specific Absorption Rate (SAR) performance (Section V), as relevant to translating this sensing technology into a wearable device in the future.

II. BREATH ACETONE SENSING USING PANI-CA STRIPS

A. Operating Principle

The proposed electromagnetic sensing mechanism is shown in Fig. 1(a) and consists of a chemo-actuating PANI-CA strip with its top fixed and its bottom free to move depending on the acetone levels, as well as a non-chemo-actuating (stationary) strip placed G_{12} away. Each of the strips has a resonant loop embedded on its bottom side, one of which is transmitting (Tx, port '1' in Fig. 1(a)) and the other receiving (Rx, port '2' in Fig. 1(a)), i.e., co-axial arrangement. As will be shown next, the dielectric properties of the stationary strip are not relevant to the design, hence we consider it as a replica of the PANI-CA strip but without chemo-actuating ability. Fig. 1(b) shows the bending angle (θ) of a 4 cm × 3 mm strip as a function of time and acetone headspace concentration. Here, we again select 4 cm × 3 mm

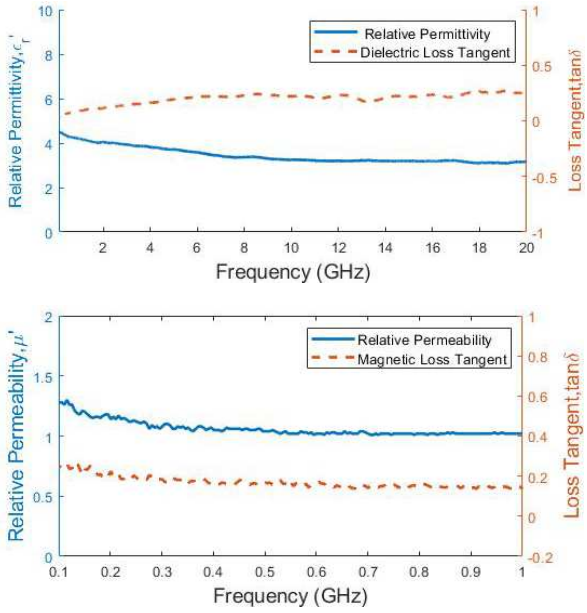

Fig. 2. Measured dielectric and magnetic properties of PANI-CA.

strips to mimic this bending performance reported in [38], i.e., θ changing from ~0º to ~30º for a headspace concentration of 0 to 1250 ppm as relevant to breath acetone sensing (see Section I). We highlight that PANI-CA strips are highly selective to acetone as compared to other gases (e.g., ethanol, 1-butanol and 2-proponal), as reported in [38].

As would be expected, loops can operate in different modes depending on the operating frequency. For instance, they are self-resonating when their circumference (C) equals the wavelength (λ) and behave as antennas. For $C < 0.1\ \lambda$, they operate in the inductive mode and for $0.1\lambda < C < \lambda$, they operate in a combined mode. As detailed in Section II.C, the inductive mode of operation is identified as optimal and capacitors are used to produce resonance and increase the transmission coefficient values ($|S_{21}|$). Specifically, as time-varying current flows through the T_x, a time-varying magnetic flux density is generated and crosses through the R_x. This induces a voltage on the R_x based upon Faraday's law of induction [40]:

$$V_{Rx} = -\frac{d}{dt}\iint B_{Tx}.\widehat{n_{Rx}}\, ds \qquad (1)$$

where, V_{Rx} is the voltage induced on the R_x, B_{Tx} is the magnetic flux density produced by the T_x, and $\hat{n}_{Rx}$ is the normal unit area vector of the R_x. As the strip bends in response to the presence of acetone, the relative position (distance) between the loops changes. That is, $\hat{n}_{Rx}$ changes, altering the induced voltage V_{Rx}. In turn, $|S_{21}|$ changes as the strip bends and can be mapped to the acetone headspace concentration. We remark that PANI-CA strips are more sensitive to acetone as compared to other VOCs [38], hence determining the accurate position of the strip in space directly relates to mapping it to the exposure level of acetone headspace concentration.

B. PANI-CA Dielectric and Magnetic Properties

To optimize our sensor design, EM properties of the PANI-CA strips need to be known. To this end, 4 cm × 3 mm

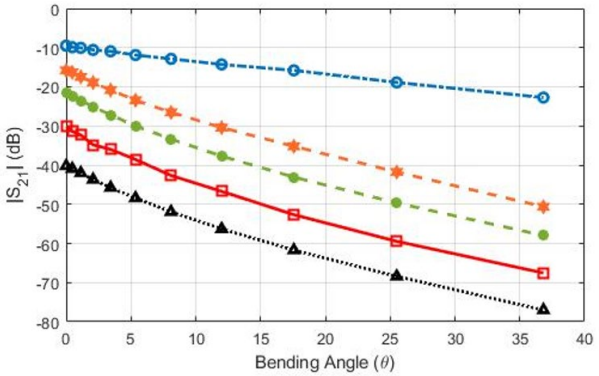

Freq (MHz)	11662	2700	950	330	220
$\lvert\Delta S_{21}\rvert$ (dB)	13.26	34.83	36.59	37.33	36.80

Fig. 3. $|S_{21}|$ as a function of bending angle for various operating frequencies in the antenna, inductive and combined modes.

PANI-CA strips are acquired (based on the fabrication process in [38]) and measured using the Keysight N1501A Dielectric Probe Kit (dielectric properties) and the Agilent E4990A with the 16454A magnetic material test fixture (magnetic properties). Measurement results are shown in Fig. 2 for the maximum frequency range allowed by each of the measurement instruments. In the 0.2 to 20 GHz range, relative permittivity ranges between 3 and 4 and dielectric loss tangent is <0.2. The material is also found to be non-magnetic. To our knowledge, this is the first time that PANI-CA dielectric/magnetic properties are reported.

C. Design Refinement

Based on the angles reported in [38], simulations are carried out in CST Microwave Studio's frequency domain solver, which employs a finite integral technique with tetrahedral meshing. The setup of Fig. 1(a) is employed with a goal to maximize resolution in capturing the PANI-CA bending (i.e., maximize the $|S_{21}|$ dynamic range, $\Delta|S_{21}|$). As a starting point, two rectangular loops of 24 mm in circumference are embedded, where the width of the loops equals that of the strip. Transmission coefficient ($|S_{21}|$) performance as a function of the strip bending angle is shown in Fig. 3 for diverse operating frequencies. Considering the breath acetone range (0º to 30°), 330 MHz exhibits the widest dynamic range of 37.33 dB. It also enables high $|S_{21}|$ values as needed to reduce the transmit power and empowered by the resonant capacitor discussed in Sec. II.A (13.7 pF in this case). An added advantage for this frequency is that it lies deep in the inductive regime such that coupling is based predominantly on magnetic fields. Since magnetic fields are transparent to non-magnetic materials (e.g., strips, biological tissues), sensor performance is not impacted by the presence or absence of such materials. As a trade off between good dynamic range and high-power requirements, we select the 330 MHz operating frequency.

Next, we proceed to refine the loop size at 330 MHz. We keep the width of the loop equal to the width of the strip and show the effect of varying loop length upon $\Delta|S_{21}|$ in Fig. 4. As seen, smaller loops improve the dynamic range (while also reducing the overall weight on the PANI-CA strip).

However, physical implementation of such small loops becomes challenging. It also shifts the $|S_{21}|$ curves to lower values, leading to higher power requirements. As a compromise, we select a loop length of 9 mm, leading to a circumference of 24 mm and a dynamic range of 37.33 dB.

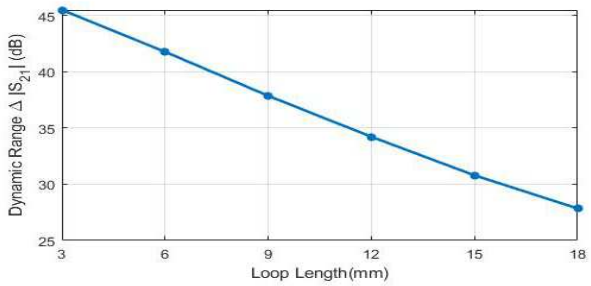

Fig. 4. $|S_{21}|$ dynamic range vs. loop length at 330 MHz

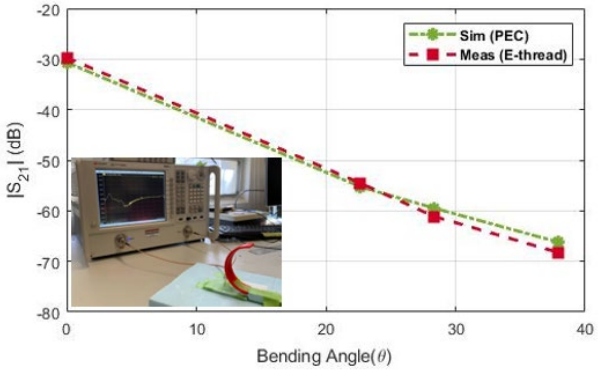

Fig. 5. Experimental validation using 3D printed fixtures and e-threads.

D. *Experimental Validation*

To fabricate the loops, 0.04-mm-diameter Elektrisola e-threads are used due to their: (a) high conductivity at the frequencies of interest [41], (b) light weight (over 4 times lighter than copper [39]) as needed to maintain bending of the PANI-CA strip with minimal obstruction, (c) mechanical flexibility for ease of fabrication, and (d) robustness (i.e., they do not delaminate, unlike conductive inks). The fabrication process can be summarized as follows. First, loops are embroidered on organza fabric using a Brother 4500D embroidery machine. This ensures shape precision and that the structure remains intact. Second, a small portion is cut off the loops and surface mount lumped capacitors are attached to achieve resonance. An additional portion is cut off to attach a 50 Ohm coaxial cable to. Third, the loops are embedded into PANI-CA strips during the casting process, and specifically when the solution is poured onto the glass slide and prior to air drying (see detailed fabrication steps for PANI-CA in [38]).

To serve as a proof-of-concept and eliminate factors affecting the natural bending of the PANI-CA strips, structures with different bending curvatures are 3D-printed to mimic the bending of PANI-CA strips per Fig. 1 [38]. Since loops operate in the deep inductive region, the presence or absence of these 3D-printed structures does not impact their performance. We remark that the goal of this setup is to validate our deformation monitoring approach

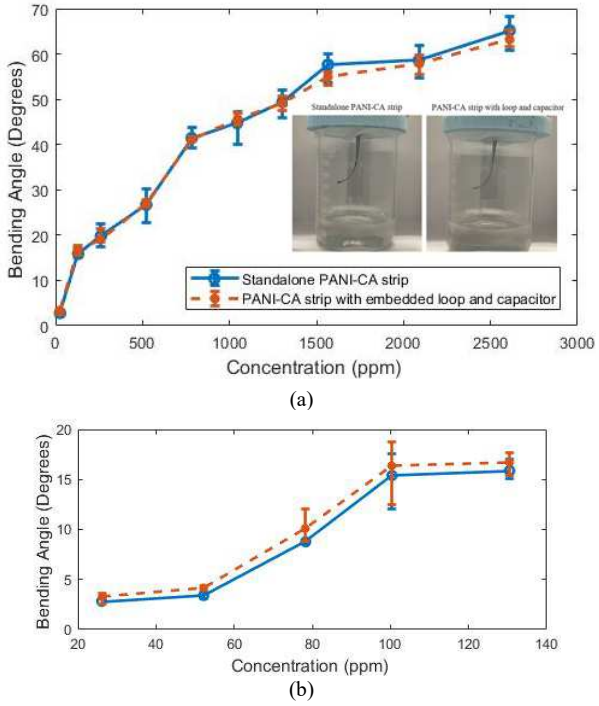

Fig. 6. Experimental validation of PANI-CA strip with embedded EM loop in presence of acetone headspace concentration.

independent of discrepancies associated with PANI-CA fabrication (e.g., strips that may not be as effective in bending) and independent of environmental influences (e.g., acetone headspace perceived by the sensor). Fig. 5 shows our measurement validation using pre-defined 3D printed fixtures. The embedded loops with capacitor are connected to a PNA-L N5235A network analyzer using co-axial cables. As seen, very good agreement is achieved between simulations and measurements. Slight discrepancies at higher bending angles are mainly due to limitations associated with the semi-rigid cables. Using flexible co-axial cables would eliminate this.

Though Fig. 5 validates the loops' ability to monitor deformation, a natural question relates to the feasibility of the PANI-CA strip to bend freely in response to acetone with the EM loop embedded within its structure. To this end, we pursue a new experimental setup where a PANI-CA strip is placed inside a 400 mL beaker and exposed to 100 mL solution with acetone concentration varying from 1% (26.1 ppm) to 100% (2610 ppm). In this case, the PANI-CA strip is allowed to move freely. Two tests are conducted: (a) stand-alone PANI-CA strip, and (b) PANI-CA strip with embedded loop and capacitor. An iPhone XR camera is fixed to a tripod stand and bending angles are recorded. Data are post-processed using MATLAB image processing tools and an in-house code to accurately track deformation. To comprehend repeatability, three separate measurements are made for each single concentration. Results are reported in Fig. 6 with the error bar displaying the highest and lowest bending angles recorded for each concentration. Referring to Fig. 6(a), the

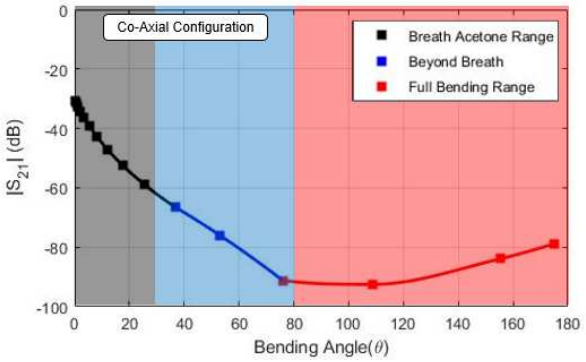

Fig. 7. Performance and utility of co-axial configuration for different application scenarios.

bending with the embedded EM loop closely resembles the standalone PANI-CA strip. The slight deviation at higher acetone headspace concentrations can be attributed to the weight on the strips and can be resolved by simply calibrating the angle vs. acetone concentration table of Fig. 1. The discrepancy can also be further reduced by employing more lightweight materials and capacitors (note that the tests of Fig. 6 use copper tape to build the loops which is two times heavier than the e-threads of Fig. 5). With EM loops embedded in PANI-CA strips, the limit of detection is 26.1 ppm, as shown in Fig. 6(b).

III. Sensor's Dynamic Range Beyond Breath Acetone Sensing

Though Fig. 3 plots $|S_{21}|$ for bending angles within the range of breath acetone deformation, Fig. 7 plots $|S_{21}|$ for bending angles up to 180º (i.e., maximum possible deformation of the strip).

Referring to Fig. 7, the grey region ($\theta<30°$) represents the sensor's performance for breath acetone sensing. In the blue region, the sensor can be used for other acetone sensing applications beyond the breath acetone range (e.g., acetone detection in non-biological settings due to its flammable nature, use of acetone as analyte during the production of certain materials). Specifically, the sensor provides a monotonic relationship between $|S_{21}|$ and bending angle up to a value of $\theta=70°$. The latter accounts for acetone gas sensing applications up to 2610 ppm (equivalent to 100% headspace concentration), as discussed in [38] and also shown in Fig. 1(b). Note that the observed trend can be physically explained via Faraday's Law in Eq. (1): as the strip deforms and distance between the two loops increases, magnetic coupling between the two reduces and $|S_{21}|$ reduces as well. However, there is a point (around 70º of deformation) where the loops' point-to-point distance increases marginally, but their orientation changes in a way that starts enhancing coupling between the two.

Should more sensitive chemo-actuating strips be developed in the future and bending exceeds 70° (even, potentially, for breath acetone) then the sensor operates in the red region and loses the monotonic relationship between $|S_{21}|$ and bending angle across the range. In summary, using the EM sensing mechanism of Fig. 1(a) on PANI-CA strips,

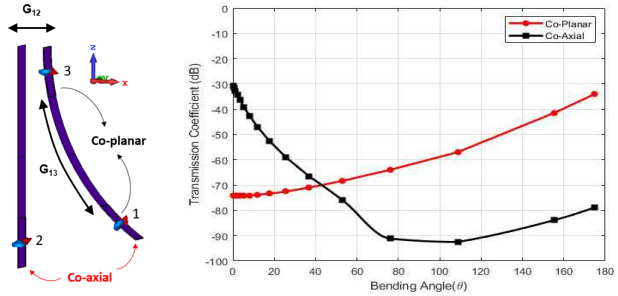

Fig. 8. Sensing technique for more sensitive chemo-actuators.

we can monitor acetone levels up to 2610 ppm, corresponding to a 70º deformation of the strip, offering an $|S_{21}|$ dynamic range of 52.62 dB. For deformation beyond 70º, alternative designs may be employed, as discussed next.

IV. Sensing of More Sensitive Chemo-Actuating Strips

To obtain precise and unambiguous deformation sensing beyond 70° of bending, an alternative design is proposed as shown in Fig. 8. In this approach, another Rx loop is placed on the PANI-CA chemo-actuator, and specifically on its top side (marked as port '3'), leading to a combination of co-axial (loops '1' and '2') and co-planar (loops '1' and '3') configurations. The transmission coefficient performance for both configurations is shown in Fig. 8 up to a bending angle of 180º. Referring to Faraday's Law in Eq. (1), for the co-planar design, the two loops get progressively closer to each other as the strip deforms with increasing acetone concentration, leading to monotonic increase of the $|S_{21}|$. Though this design can be used as stand-alone, it is significantly limited in dynamic range as compared to the co-axial design. For example, for $\theta<30°$ (i.e., breath acetone range) $\Delta|S_{21}| = 26.35$ dB and $\Delta|S_{31}| = 1.79$ dB for the co-axial and co-planar designs, respectively. For $\theta<70°$ (blue zone in Fig. 7) $\Delta|S_{21}| = 25.75$ dB and $\Delta|S_{31}| = 6.75$ dB. This difference in dynamic range between the two configurations is again related to the geometry of the structure and the difference in coupling dictated by Faraday's Law: for the co-planar case, the relative displacement of the loops is much more pronounced as compared to the co-axial case, leading to wider dynamic range. Hence, the co-axial design was analyzed in Section II and combinations of the three loops are herewith proposed to eliminate ambiguities should a strip deformation of beyond 70º needs to be monitored. Notably, experiments similar to those discussed in Fig. 6 show that the addition of a second loop upon the strip restricts its range of motion by less than 0.5º which can be easily calibrated. To further elucidate the differences between co-axial and co-planar designs, we analyze some realistic scenarios next:

1) Bending of PANI-CA strip with time. As noted in [38], PANI-CA strips bend in a reversible process. Thus, it is essential to understand the performance of the proposed EM-mechanism using PANI-CA chemo-actuators *vs.* time. For a scenario when the sensor is exposed to 100% acetone concentration (equivalent to 2610 ppm), the PANI-CA strip bends to a maximum of $\theta=68°$ in 55 sec and recoils to its original position in 50 sec. Fig. 9(a) shows the simulated response of the sensor with time for both co-planar and co-

axial scenarios. The simulated dynamic range for co-planar design is 8.22 dB while for co-axial design it is 52.62 dB.

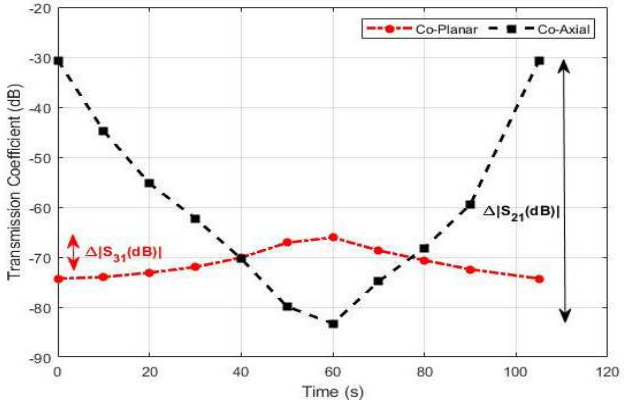

(a)

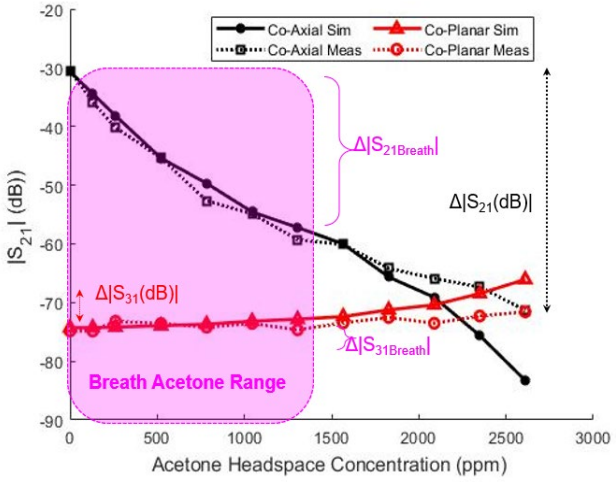

(b)

Fig. 9. Ability of the sensor to monitor bending of the PANI-CA strip (a) with time (simulated), and (b) with acetone headspace concentration (simulated and measured).

2) Bending of PANI-CA strip with acetone headspace concentration. PANI-CA strips acquired from the authors in [38] are embedded with loops and capacitors and connected to a network analyzer using thin, U.FL co-axial cables. The strips are free to move inside a 400 mL beaker with 100 mL acetone solution mimicking concentrations from 0 to 2610 ppm. When maximum bending is achieved, the corresponding transmission coefficient values are recorded using the network analyzer. Measurement results are shown in Fig. 9(b) and compared against simulations. In the breath acetone detection range highlighted in pink, the standalone co-planar design in simulation (represented as Co-planar Sim.) yields a dynamic range of 1.79 dB. In measurements, the dynamic range achieved is 1.37 dB. The dynamic range achieved in simulation using a standalone co-axial design (represented as Co-axial Sim.) is 26.35 dB. In measurements, it is 26.158 dB. That is, we have great agreement between simulations and measurements and ~19 times better dynamic range for co-axial vs. co-planar design.

Referring to the inset of Fig. 9(b), the co-axial design also achieves excellent resolution at lower acetone concentrations. Using this, we interpolated the results to find the change in $|S_{21}|$ that achieves a resolution of 1 ppm of acetone headspace. We concluded that 1 ppm of acetone headspace concentration yields a change in $|S_{21}|$ by 0.05 dB, meaning that a receiver with two decimal places of resolution can monitor up to 1 ppm change in acetone headspace concentration. Increasing the receiver resolution or improving the sensitivity of PANI-CA strips can improve this detection limit.

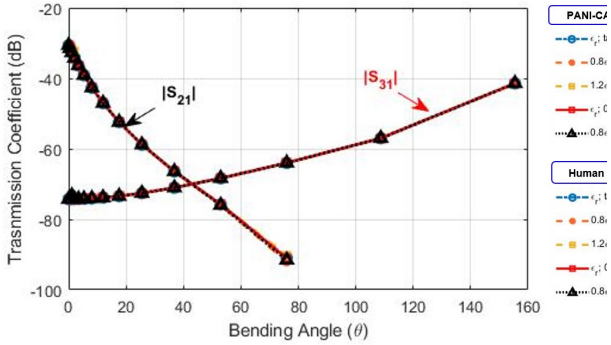

Fig. 10. Change in transmission coefficient ($|S_{21}|$ and $|S_{31}|$) with ±20% variation in permittivity (ε_r) and loss tangent ($\tan\delta$) of the PANI-CA strip and human tissue properties.

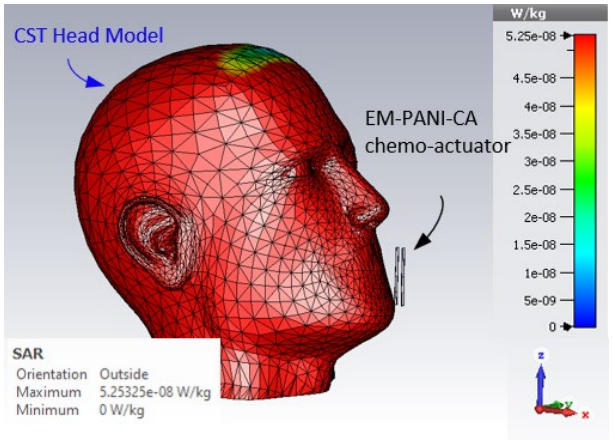

Fig. 11. Analysis of Specific Absorption Rate (SAR) in proximity to a human head model for a potential breathalyzer application.

V. Other Considerations

A. Sensitivity to surrounding dielectric materials

In a real deployment scenario, the sensor would be surrounded by various dielectric media, including the PANI-CA polymer and biological tissues. As would be expected, the sensor must be insensitive to variations in the dielectric properties of such materials. Its operation deep in the inductive regime is beneficial to this end, as also highlighted in Section II.C. To validate this, the sensor is simulated in proximity to a homogeneous human head model and dielectric properties of both the PANI-CA strip and tissues are varied by ±20% from their nominal values. Simulation results in Fig. 10 confirm the sensor's robustness.

B. Specific Absorption Rate (SAR)

Specific Absorption Rate (SAR) investigations are carried out to guarantee compliance with international safety criteria. Again, a homogeneous head model is employed with

the sensor of Fig. 8 placed in close proximity to the mouth. The input power to the transmitting loop is set to -15 dBm (31.62 μW) and the SAR averaged over 1 g of tissue is plotted in Fig. 11. As seen, the highest value is 0.0525 μW/Kg, which is significantly less than the Federal Communications Commission (FCC) limit of 1.6 W/Kg.

VI. Conclusion

This paper described a novel approach for monitoring breath acetone levels as a biomarker of human metabolism. The proposed electromagnetic sensing mechanism integrates chemo-actuating PANI-CA strips with resonant loops and relies on electromagnetic principles to monitor deformation and, hence, breath acetone levels. Proof-of-concept simulations and *in vitro* experimental results were carried out to demonstrate feasibility, optimize the design, explore scalability to various acetone levels and strip deformations, and address practical considerations. Unlike prior technologies, the proposed technique has the potential to be used continuously to monitor acetone levels at room temperature and can be ultimately integrated into a wearable device. We determined the detection limit to be 26.1 ppm experimentally for the current setup and extrapolated the results to demonstrate the feasibility of detecting as low as 1 ppm. Because the technology is insensitive to surrounding dielectric materials, it is robust to changes in tissue dielectric properties.

Future research will focus on developing an integrated sensor incorporated into a wearable device (such as mask or mouthpiece), *in vivo* validation, and resolution enhancement with advances on the materials side of the PANI-CA strip. The technology can ultimately be applied to a variety of health diagnostic applications, including metabolic-rate activity sensing, weight loss, and ketosis.

Acknowledgment

The authors would like to express their gratitude to Dr. Pelagia-Iren Gouma and her team for providing PANI-CA actuators for material analysis and experimental studies for concept validation.

References

[1] J. Moore, N. Chaudhary and T. Akinyemiju, "Metabolic Syndrome Prevalence by Race/Ethnicity and Sex in the United States, *National Health and Nutrition Examination Survey*, 1988–2012", 2021.

[2] G. Hirode and R. Wong, "Trends in the Prevalence of Metabolic Syndrome in the United States, 2011-2016", *JAMA*., vol. 323, no. 24, p. 2526, 2020. Available: 10.1001/jama.2020.450.

[3] N.O. E. Initiative, "Clinical Guidelines on the identification, evaluation, and treatment of overweight and obesity in adults," *National Heart, Lung, and Blood Institute*, 1998

[4] UF Health: University of Florida Health [Internet]. Gainesville (FL): University of Florida Health; c2022. Comprehensive metabolic panel: Overview; [updated 2021 Jan 24; cited 2021 Feb 14]; [about 2 screens]. Available from: https://ufhealth.org/comprehensive-metabolic-panel

[5] C. Compher, D. Frankenfield, N. Keim and L. Roth-Yousey, "Best Practice Methods to Apply to Measurement of Resting Metabolic Rate in Adults: A Systematic Review", *Journal of the American Dietetic Association*, vol. 106, no. 6, pp. 881-903, 2006.

[6] C. Turner, B. Parekh, C. Walton, P. Spanl, D. Smith and M. Evans, "An exploratory comparative study of volatile compounds in exhaled breath and emitted by skin using selected ion of tube mass spectrometry," *Rapid Commun. Mass Sp.*, vol. 22, pp. 526–532, 2008.

[7] T. Tsuda, T. Ohkuwa, and H. Itoh, "Findings of skin gases and their possibilities in healthcare monitoring," in Yoshikawa T, Naito Y (eds): *Gas Biology Research in Clinical Practice*. Basel, Karger, 2011, pp 125–132 (DOI:10.1159/000321953).

[8] S. K. Kundu, R. W. George, S. C. March, and S. Rutnarak, "Method and device for ketone measurement," *ed: Google Patents*, 1991

[9] H.H. Huang, et al., "A highly sensitive QCM sensor coated with Ag+-ZSM-5 film for medical diagnosis," *Sens. Actuators*, B, vol. 101, no. 3, pp. 316-321, 2004.

[10] N. Yamane, T. Tsuda, K. Nose, et al., "Relationship between skin acetone and blood β-hydroxybutyrate concentrations in diabetes," *Clinica Chimica Acta*, vol. 365, pp. 325-329, 2006.

[11] T. Ohkuwa, T. Funada, and T. Tsuda, "Acetone response with exercise intensity," Advanced Gas Chromatography – *Progress in Agricultural, Biomedical and Industrial Applications*, *InTechOpen*, pp. 151-160, 2012.

[12] K. Yamai, T. Ohkuwa, H. Itoh, Y. Yamazaki, and T. Tsuda, "Influence of cycle exercise on acetone in expired air and skin gas," *Redox Report Communications in Free Radical Research*, vol. 14, no. 6, pp. 185-289, 2009.

[13] J.C. Anderson, "Measuring breath acetone for monitoring fat loss: Review," *Obesity Biology and Integrated Physiology*, vol. 23, no. 12, pp. 2327-2334, 2015.

[14] K. Mori, T. Funada, M. Kikuchi, T. Ohkuwa, H. Itoh, Y. Yamazaki, et al., "Influence of dynamic hand-grip exercise on acetone in gas emanating from human skin," *Redox Report*, vol. 13, pp. 139-142, 2008.

[15] J. Anderson, "Measuring breath acetone for monitoring fat loss: Review", Obesity, vol. 23, no. 12, pp. 2327-2334, 2015. Available: 10.1002/oby.21242 [Accessed 15 April 2022].

[16] S. Massick, "Portable breath acetone measurements combine chemistry and spectroscopy", SPIE Newsroom, 2007. Available: 10.1117/2.1200712.0948.

[17] H. Schwoebel et al., "Phase-resolved real-time breath analysis during exercise by means of smart processing of PTR-MS data", Analytical and Bioanalytical Chemistry, vol. 401, no. 7, pp. 2079-2091, 2011. Available: 10.1007/s00216-011-5173-2

[18] C. Turner, P. Španěl and D. Smith, "A longitudinal study of ammonia, acetone and propanol in the exhaled breath of 30 subjects using selected ion flow tube mass spectrometry, SIFT-MS", Physiological Measurement, vol. 27, no. 4, pp. 321-337, 2006. Available: 10.1088/0967-3334/27/4/001 [Accessed 15 March 2022].

[19] L. Wang, "Tailored Synthesis and Characterization of Selective Metabolite-detecting nanoprobes for Handheld Breath Analysis", Ph.D, Stony Brook University, 2008.

[20] R. Centeno, J. Mandon, F. Harren and S. Cristescu, "Influence of Ethanol on Breath Acetone Measurements Using an External Cavity Quantum Cascade Laser", Photonics, vol. 3, no. 2, p. 22, 2016. Available: 10.3390/photonics3020022

[21] L. Ciaffoni et al., "Demonstration of a Mid-Infrared Cavity Enhanced Absorption Spectrometer for Breath Acetone Detection", Analytical Chemistry, vol. 85, no. 2, pp. 846-850, 2012. Available: 10.1021/ac3031465 [Accessed 10 August 2022].

[22] F. Nadeem, J. Mandon, A. Khodabakhsh, S. Cristescu and F. Harren, "Sensitive Spectroscopy of Acetone Using a Widely Tunable External-Cavity Quantum Cascade Laser", Sensors, vol. 18, no. 7, p. 2050, 2018. Available: 10.3390/s18072050.

[23] E. Wongrat, N. Chanlek, C. Chueaiarrom, W. Thupthimchun, B. Samransuksamer and S. Choopun, "Acetone gas sensors based on ZnO nanostructures decorated with Pt and Nb", Ceramics International, vol. 43, pp. S557-S566, 2017. Available: 10.1016/j.ceramint.2017.05.296.

[24] J. Hu et al., "One-step synthesis of 2D C3N4-tin oxide gas sensors for enhanced acetone vapor detection", Sensors and Actuators B: Chemical, vol. 253, pp. 641-651, 2017. Available: 10.1016/j.snb.2017.06.176.

[25] L. Ma et al., "PrFeO3 hollow nanofibers as a highly efficient gas sensor for acetone detection", Sensors and Actuators B: Chemical, vol. 255, pp. 2546-2554, 2018. Available: 10.1016/j.snb.2017.09.060.

[26] F. Liu et al., "Sub-ppm YSZ-based mixed potential type acetone sensor utilizing columbite type composite oxide sensing electrode",

Sensors and Actuators B: Chemical, vol. 238, pp. 928-937, 2017. Available: 10.1016/j.snb.2016.06.171

[27] S. Navale et al., "Enhanced acetone sensing properties of titanium dioxide nanoparticles with a sub-ppm detection limit", Sensors and Actuators B: Chemical, vol. 255, pp. 1701-1710, 2018. Available: 10.1016/j.snb.2017.08.186.

[28] L. Wang and P. Gouma, "Selective Crystal Structure Synthesis and Sensing Dependencies", *Metal Oxide Nanomaterials for Chemical Sensors*, pp. 167-188, 2012.

[29] K. Khorsand Kazemi et al., "Low-Profile Planar Antenna Sensor Based on Ti 3 C 2 T x MXene Membrane for VOC and Humidity Monitoring", Advanced Materials Interfaces, vol. 9, no. 13, p. 2102411, 2022.

[30] A. Javadian-Saraf, E. Hosseini, B. Wiltshire, M. Zarifi and M. Arjmand, "Graphene oxide/polyaniline-based microwave split-ring resonator: A versatile platform towards ammonia sensing", Journal of Hazardous Materials, vol. 418, p. 126283, 2021. Available: 10.1016/j.jhazmat.2021.126283

[31] H. Li et al., "Multi-frequency measurement of volatile organic compounds with a radio-frequency interferometer," IEEE Sensors J., vol. 17, no. 11, pp. 3323–3331, Jun. 2017.

[32] W. T. Chen, K. M. E. Stewart, R. R. Mansour, and A. Penlidis, "Polymeric sensing material-based selectivity-enhanced RF resonant cavity sensor for volatile organic compound (VOC) detection," in IEEE MTT-S Int. Microw. Symp. Dig., May 2015, pp. 1–3

[33] S. Mohammadi and M. H. Zarifi, "Differential Microwave Resonator Sensor for Real-Time Monitoring of Volatile Organic Compounds," in IEEE Sensors Journal, vol. 21, no. 5, pp. 6105-6114, 1 March1, 2021, doi: 10.1109/JSEN.2020.3041810.

[34] "Home", KETONIX Breath Ketone Analyzer, 2022. [Online]. Available: https://www.ketonix.com/. [Accessed: 02- Mar- 2022].

[35] "The most effective weight loss program - Keyto", Keyto, 2022. [Online]. Available: https://getkeyto.com/. [Accessed: 02- Mar- 2022].

[36] "Biosense. Readout Health, Biosense™. Available online: https://mybiosense.com/. [Accessed: 03- Mar- 2022].

[37] A. Reed, "5 Best Ketone Breath Meters in 2022 [+Beginner's Guide] |Bodyketosis", Bodyketosis, 2022. [Online]. Available: https://bodyketosis.com/ketone-breath-analyzer/. [Accessed: 16- Mar- 2022].

[38] Mojtabavi M., Jodhani G., Rao R., Zhang J. & Gouma Pl., A PANI–Cellulose acetate composite as a selective and sensitive chemomechanical actuator for acetone detection, *Advanced Device Materials*, 2:1, 1-7, (2016)

[39] V. Mishra and A. Kiourti, "Electromagnetic Components Realized on Conductive Wires: A Copper vs. E-Thread Comparison," 2019 IEEE International Symposium on Antennas and Propagation and USNC-URSI Radio Science Meeting, 2019, pp. 359-360

[40] W. H. Hayt, Jr. and J. A. Buck, "Time-varying fields and Maxwell's equations," in Engineering Electromagnetics, 6th ed.NewYork,NY, USA: McGraw-Hill, 2001.

[41] A. Kiourti, C. Lee, and J.L. Volakis, "Fabrication of Textile Antennas and Circuits with 0.1mm Precision," IEEE Antennas and Wireless Propagation Letters, vol. 15, pp. 151-153, 2016.